BBA - Molecular Basis of Disease xxx (2016) xxx-xxx

Contents lists available at ScienceDirect

BBA - Molecular Basis of Disease

journal homepage: www.elsevier.com

Challenging drug target for Parkinson's disease: Pathological complex of the chameleon TPPP/p25 and alpha-synuclein proteins

Tibor Szénási [a, 1], Judit Oláh [a, 1], Adél Szabó [a], Sándor Szunyogh [a], András Láng [b], András Perczel [b, c], Attila Lehotzky [a], Vladimir N. Uversky [d, e], Judit Ovádi [a, *]

[a] Institute of Enzymology, Research Center for Natural Sciences, Hungarian Academy of Sciences, Budapest 1117, Hungary
[b] MTA-ELTE, Protein Modelling Research Group, Institute of Chemistry, Eötvös Loránd University, Budapest 1117, Hungary
[c] Laboratory of Structural Chemistry and Biology, Institute of Chemistry, Eötvös Loránd University, Budapest 1117, Hungary
[d] Department of Molecular Medicine and USF Health Byrd Alzheimer's Research Institute, Morsani College of Medicine, University of South Florida, 33612 Tampa, FL, USA
[e] Laboratory of Structural Dynamics, Stability and Folding of Proteins, Institute of Cytology, Russian Academy of Sciences, St. Petersburg, Russia

ARTICLE INFO

Article history:
Received 30 June 2016
Received in revised form 2 September 2016
Accepted 20 September 2016
Available online xxx

Keywords:
Tubulin Polymerization Promoting Protein/p25
α-Synuclein
Deletion mutants
Protein chameleon
Drug target
Bimolecular fluorescence complementation

ABSTRACT

The hallmarks of Parkinson's disease and other synucleinopathies, Tubulin Polymerization Promoting Protein (TPPP/p25) and α-synuclein (SYN) have two key features: they are disordered and co-enriched/co-localized in brain inclusions. These *Neomorphic Moonlighting Proteins* display both physiological and pathological functions due to their interactions with distinct partners. To achieve the selective targeting of the pathological TPPP/p25-SYN but not the physiological TPPP/p25-tubulin complex, their interfaces were identified as a specific innovative strategy for the development of anti-Parkinson drugs. Therefore, the interactions of TPPP/p25 with tubulin and SYN were characterized which suggested the involvements of the 178–187 aa and 147–156 aa segments in the complexation of TPPP/p25 with tubulin and SYN, respectively. However, various truncated and deletion mutants reduced but did not abolish the interactions except one mutant; in addition synthetized fragments corresponding to the potential binding segments of TPPP/p25 failed to interact with SYN. In fact, the studies of the multiple interactions at molecular and cellular levels revealed the high conformational plasticity, *chameleon* feature, of TPPP/p25 that ensures exceptional functional resilience; the lack of previously identified binding segments could be replaced by other segments. The experimental results are underlined by distinct bioinformatics tools. All these data revealed that although targeting *chameleon* proteins is a challenging task, nevertheless, the validation of a drug target can be achieved by identifying the interface of complexes of the partner proteins existing at the given pathological conditions.

1. Introduction

The sensing, integrating and coordinating features of eukaryotic cells are achieved by complex ultrastructural arrays and multifarious functions of the cytoskeletal network that comprises networks of fibrous proteins in a form of microtubules, actin and intermediate filaments. These filamentous polymer structures are highly dynamic and undergo constant and rapid reorganization during cellular life cycle. The microtubule system plays a crucial role in brain physiology, as it is involved in an enormous number of cellular events including cell differentiation and pathological inclusion formation [1,2]. These various functions of microtubules are achieved by their decoration with proteins/enzymes that exert specific effects on the dynamics and the organization of the cytoskeleton resulting in distinct functions with *moonlighting* features [3]. Moonlighting proteins perform multiple independent functions originated not from alterations at gene level, but because of the consequence of altered cellular localization, oligomeric states or distinct interacting partners [4]. In the case of *neomorphic moonlighting* proteins [5], the physiological function can be converted into a pathological one due to interaction with a different partner protein in the pathological milieu. The prototype of these *neomorphic moonlighting* proteins is the Tubulin Polymerization Promoting Protein (TPPP/p25) [6].

TPPP/p25 is a Microtubule Associated Protein; its expression is finely controlled in the human brain [7–9]. It is an intrinsically disordered protein (IDP) without a well-defined 3D structure, whose middle, highly flexible CORE region is straddled by the unstructured *N*- and *C*-termini [10]. TPPP/p25 modulates the dynamics and stability of the microtubule system, where it is primarily engaged in the development of projections of oligodendrocytes that are responsible for the ensheathment of axons [7,9,11]. A couple of specific binding domains in the disordered TPPP/p25 have been identified both sequentially and experimentally such as a zinc finger motif, consensus GTP binding domain, phosphorylation sites, and the functional consequences of these sites have been established ([12] and references therein). The non-physiological expression levels of this IDP lead to

* Corresponding author at: Institute of Enzymology, Research Center for Natural Sciences, Hungarian Academy of Sciences, Magyar tudósok körútja 2, H-1117 Budapest, Hungary.
Email addresses: szenasi.tibor@ttk.mta.hu (T. Szénási); olah.judit@ttk.mta.hu (J. Oláh); szabo.adel@ttk.mta.hu (A. Szabó); szunyogh.sandor@ttk.mta.hu (S. Szunyogh); langax@chem.elte.hu (A. Láng); perczel@chem.elte.hu (A. Perczel); lehotzky.attila@ttk.mta.hu (A. Lehotzky); vuversky@health.usf.edu (V.N. Uversky); ovadi.judit@ttk.mta.hu (J. Ovádi)

[1] These two authors contributed equally to the work.

http://dx.doi.org/10.1016/j.bbadis.2016.09.017
0925-4439/

distinct CNS diseases such as glioma (brain tumor) [13], multiple sclerosis (demyelination) [14,15] or synucleinopathies (pathological inclusions) [16]. In fact, TPPP/p25 is able to induce α-synuclein (SYN) aggregation [17] in vitro; however, its overexpression and co-localization with SYN in human brain is a characteristic symptom of Parkinson's disease [16], thus we have suggested TPPP/p25 as a biomarker of synucleinopathies [16]. Nevertheless, we have also detected TPPP/p25 and SYN-enriched inclusions in the case of diffuse Lewy body dementia with Alzheimer's disease as well [18].

The disordered SYN is considered as a classic *chameleon* protein [19]. Similarly as chameleons change color to mimic their environment, protein chameleons have high structural plasticity and are able to adopt various conformations in a template-dependent manner [19]. Although the intrinsically disordered SYN is predominantly unfolded at physiological conditions, in response to changes in its environment it is capable of adopting structurally unrelated conformations ranging from intrinsically disordered form to various partially folded conformations with different contents of secondary structural elements induced by low pH, high temperature, organic solvents, membranes, agrochemicals, or metal ions [19,20]. The structural properties of SYN have been extensively characterized under a variety of conditions [21–29]. Despite the fact that the unstructured *C*-terminal segment (45 aa) is involved in the modulation of SYN aggregation at extreme in vitro conditions, yet a terminal 30-residue-long peptide was found to be ineffective as a competitor in aggregation processes, indicating its chameleon nature [19].

Although knowledge on various mechanisms underlying Parkinson's disease and other synucleinopathies has been greatly expanded over the last decades, the pathomechanism is still not well-understood [30–32]. Different mechanisms have been suggested such as mitochondrial dysfunction, cytoskeletal alterations, enhanced oxidative stress or impairment of protein clearance pathways. SYN plays multiple pivotal roles in these diseases, nowadays its small, soluble oligomeric forms with beta-sheet conformation are considered the most toxic species [30,32,33]. To target SYN toxicity, the current strategies focus on its increased expression level (by gene silencing), aggregation (by anti-aggregation compounds), defective clearance (by autophagy inducers), and/or cell-to-cell propagation of its neurotoxic conformers (by immunotherapy, degrading enzymes) [30,34].

Recently we have suggested a new strategy for the therapeutic treatment of Parkinson's disease by targeting the interface of the pathological TPPP/p25-SYN complex without influencing the physiological interaction of TPPP/p25 with tubulin/microtubules [35,36]. The distinct interface of the physiological and pathological complexes is a crucial point in our drug targeting strategy. Our analysis revealed that the ^{147}KAPIISGVTK^{156} segment in the flexible CORE region of TPPP/p25 and the ^{126}EMPSEEGYQDYEPEA^{140} segment of the *C*-terminus of SYN are involved in the formation of the interface of their pathological complex [36]. Massive intracellular aggregation of the *N*- and *C*-terminally-truncated TPPP/p25 and SYN or its fragments was established. This finding initiated our research aiming at the elucidation of the nature of the TPPP/p25-SYN interaction, in order to better understand how these two disordered proteins generate oligomeric, soluble pathological associates acting as the fatal species that lead to the development of inclusions observed under pathological conditions.

It has been documented that these small, soluble and highly expressed *moonlighting* proteins are unstructured under physiological conditions, and they frequently display multiple functions due to their conformational plasticity and their ability to *act as protein chameleons* [19]. In this work, we established the *chameleon* nature of TPPP/p25 using various truncated and deletion mutants/fragments in the interaction and functional studies and revealed a main challenge associated with the design of drugs targeting such *chameleon* proteins.

2. Materials and methods

2.1. Antibodies, peptides

The following antibodies were used: mouse monoclonal tubulin antibody (Sigma T9026, clone DM1A), mouse monoclonal SYN antibody against the epitope of 121–125 aa (Sigma S5566, clone Syn211) and rat polyclonal TPPP/p25 antibody [16]. The peptides BF181–183 were synthesized as described in [35].

2.2. DNA manipulations

The internal single and discontinue deletion mutants of TPPP/p25 were constructed by a polymerase chain reaction (PCR) based on overlap extension method [37] as described below. The first PCR generated two fragments using two pairs of primers: primer1 (forward) and primer2 (reverse) or primer5 (reverse) or primer7 (reverse) or primer9 (reverse) or primer11 (reverse) and primer3 (forward) or primer6 (forward) or primer8 (forward) or primer10 (forward) or primer12 (forward) and primer4 (reverse) and pET21c–TPPP/p25 as a template (Table 1).

The two fragments were then used as the template for a second PCR with primer pair primer1 (forward) and primer4 (reverse). The fragments obtained from the second PCR were inserted into the NdeI/XhoI sites of pET21c to generate the Δ 147–156 TPPP/p25 (SL) or Δ 142–162 TPPP/p25 (LL) or Δ 59–62 TPPP/p25 (ML) or Δ 178–187 TPPP/p25 (TL) or Δ 112–144 TPPP/p25 (CL) mutants (Table 2). For the double deletion mutant (DL), the first PCR generated two fragments using two pairs of primers: primer1 (forward) and primer7 (reverse) and primer8 (forward) and primer4 (reverse) and SL as a template.

The double truncated TPPP/p25 (pET21c–TPPP/p25 Δ3–43/Δ175–219, DT) was prepared and purified as described previously [35]. The double truncated mini loop TPPP/p25 (DTML), double truncated small loop TPPP/p25 (DTSL) and double truncated double loop TPPP/p25 (DTDL) were amplified by PCR using the following primer pairs: primer13 and primer17 and ML, SL or DL as a template. After digestion with *Nde*I and *Xho*I restriction enzymes, inserts were ligated into pET21c vector (Novagen).

The human TPPP/p25 peptides corresponding to residues 43–90 (rfr-1) and 142–187 (rfr-2) with a His-tag were amplified by PCR using forward primer primer13 or primer15 and reverse primer primer14 or primer16 and human full length TPPP/p25 plasmid [11] as a template. After digestion with NdeI and XhoI restriction enzymes, inserts were ligated into pET15b vector (Novagen). The human TPPP/p25 peptide corresponding to residues 142–219 *C*-terminal without 178–187 segment (rfr-3) with a His-tag was amplified by PCR using primer15 (forward) and primer4 (reverse) with TL plasmid as a template. Correct insertion of all these plasmids was verified by DNA sequencing.

2.3. Bimolecular fluorescence complementation (BiFC) plasmids

The BiFC plasmids (pBiFC-VN1–173, pBiFC-VC155–238) were the gift of Prof. Péter Várnai (Semmelweis University, Budapest). To insert the full length TPPP/p25 cDNA in either the pBiFC-VN1–173 or pBiFC-VC155–238 the following primers for PCR amplification

Table 1
TPPP/p25 primers.

Short name	Long name	Primer sequence
primer1	TPPP/p25 5′ wt F	AGATACACATATGGCTGACAAGGCTAAGC
primer2	Δ 147–156 TPPP/p25 R	GGGCGACGAGATGGCGCCCTCGATGAGCCTGTG
primer3	Δ 147–156 TPPP/p25 F	AGGCTCATCGAGGGCGCCATCTCGTCGCCCACAG
primer4	TPPP/p25 3′ wt R	GTGCTCGAGCTTGCCCCCTTGC
primer5	Δ 142–161 TPPP/p25 R	GAGGTTCGCGAGGTGCACACAGTGTCGAGGCTC
primer6	Δ 142–161 TPPP/p25 F	CGTTCGCGAGGTGCACACAGTGTCGAGGCTCACG
primer7	Δ 59–62 TPPP/p25 R	TCCCGGTGGCCCTGGCGTCAAAGCGCCGGAAGGCCTCCTC
primer8	Δ 59–62 TPPP/p25 F	AGGAGGCCTTCCGGCGCTTTGACGCCAGGGCCACCGGGAG
primer9	Δ 178–187 TPPP/p25 R	CACGCGGCCAGCCTTGCCCTTGTGGGAGCCCGTGAAC
primer10	Δ 178–187 TPPP/p25 F	ACGGGCTCCCACAAGGGCAAGGCTGGCCGCGTGGATC
primer11	Δ 112–144 TPPP/p25R	GATGATGGGCGCCTTGCCCTCGGTGATGGTCCGGCAAGACTTC
primer12	Δ 112–144 TPPP/p25 F	GAAGTCTTGCCGGACCATCACCGAGGGCAAGGCGCCCATCATC
primer13	TPPP/p25 truncated F	GAGATATACATATGGCTGCATCCCCTGAGCTC
primer14	43–90 TPPP/p25 R	TGACCTCGAGGTTCCTGCCGTCGATCACCTGG
primer15	142–187 TPPP/p25 F	GAGCATATGAGGCTCATCGAGGGCAAGGCGCCC
primer16	142–187 TPPP/p25 R	AGCCTCGAGCTTGCCCTTGCCAGAGGGGTCGAAGCGC
primer17	TPPP/p25 truncated R	GGTGCTCGAGGCCCGTGAACTTGGTGGTGTC

Table 2
TPPP/p25 variants: truncated and deletion mutants as well as fragments.

	Long name	Sequence	Abbreviation
1	Full length	**1–219**	***FL***
2	Mini loop	**Δ59–62**	***ML***
3	Small loop	**Δ147–156**	***SL***
4	Double loop	**Δ59–62/Δ147–156**	***DL***
5	Large loop	**Δ142–161**	***LL***
6	Tubulin loop	**Δ178–187**	***TL***
7	Central loop	**Δ112–144**	***CL***
8	Double truncated	**Δ3–43/Δ175–219**	***DT***
9	Double truncated mini loop	**Δ3–43/Δ175–219 + Δ59–62**	***DTML***
10	Double truncated small loop	**Δ3–43/Δ175–219 + Δ147–156**	***DTSL***
11	Double truncated double loop	**Δ3–43/Δ175–219 + Δ59–62/Δ147–156**	***DTDL***
12	Recombinant fragment 1	**43–90**	***rfr-1***
13	Recombinant fragment 2	**142–187**	***rfr-2***
14	Recombinant fragment 3	**142–219, Δ178–187**	***rfr-3***

were used: 5-GAAGGAGCTCGAGATATGGCTGACAAGGCTAAGC-3 (forward) and 5-CCGTGGATCCCTACTTGCCCCCTTGCACCTTCTGGTCGTAGG-3 (reverse). The PCR product, following purification and after digestion with *Xho*I-*Bam*HI restriction enzymes, was inserted to XhoI and BamHI sites in the BiFC vectors. To insert the full length SYN cDNA in either the pBiFC-VN1–173 or pBiFC-VC155–238, the following primers for PCR amplification were used: 5-ATCTCGAGGCATGGATGTATTCATGAAAGG-3 (forward) and 5-AGAAGATCTTTAGGCTTCAGGTTCGTAGTCTTGATACC-3 (reverse). The PCR product, following purification and after digestion with XhoI-*Bgl*II restriction enzymes, was inserted to XhoI and BamHI sites in the BiFC vectors. The sequences of all construct were verified by restriction mapping and sequencing.

2.4. Expression and purification of human recombinant wild type and mutant TPPP/p25 forms

Human recombinant TPPP/p25 forms and fragments (see Table 2) possessing His-tags were expressed in *E. coli* BL21 (DE3) cells and isolated on HIS-Select™ Cartridge (Sigma-Aldrich) as described previously [16,35].

In the case of LL, the purification was based on the method described in [38]. Briefly, the cell pellet was resuspended in buffer A (10 mM tris(hydroxymethyl)aminomethane (Tris), 100 mM phosphate buffer pH 7.5 containing 50 mM NaCl) with 10 μM 4-(2-aminoethyl) benzenesulfonyl fluoride hydrochloride, 1 mM benzamidine, 1 μg/ml pepstatin, 1 μg/ml leupeptin and 1 mg/ml lysozyme (Sigma L7651); and further lysed by sonication. After centrifugation (25 min, 4 °C, 20,000 g), the pellet was resuspended in buffer A containing 1 M urea and 1% Triton X-100. After centrifugation (25 min, 4 °C, 20,000 g), the pellet was resuspended in buffer A containing 8 M guanidine·HCl, sonicated and centrifuged again (25 min, 4 °C, 20,000*g*). The final supernatant was diluted two-fold with buffer A, and loaded to a HIS-Select™ Cartridge (Sigma P6611) equilibrated with buffer A. After extensive washing, the protein was eluted with 50 mM Na-acetate buffer pH 4.5 containing 150 mM NaCl. The eluted fractions were concentrated with a YM10 Diaflo membrane (Amicon, Danvers, MA), dialyzed overnight in 50 mM NH_4-acetate, lyophilized and stored at − 80 °C.

The purity of proteins was analyzed by sodium dodecyl sulfate polyacrylamide gel electrophoresis (SDS-PAGE).

Protein concentrations of the TPPP/p25 variants were determined on the basis of the absorbance at 280 nm using the extinction coefficients evaluated by ProtParam [39], 10,095 M^{-1} *cm^{-1} for full length TPPP/p25, ML, SL, DL, LL, TL, CL; 5625 M^{-1} *cm^{-1} for DT, DTML, DTSL, DTDL, rfr-1, and 4470 M^{-1} *cm^{-1} for rfr-3, respectively. Since rfr-2 does not contain any Trp, Tyr or Phe, its concentration was determined by the Bradford method [40].

2.5. Tubulin and SYN preparation

Tubulin was prepared from bovine brain according to the method of Na and Timasheff [41]. Human recombinant SYN was prepared as described previously [42]. SYN concentration was determined from the absorbance at 280 nm using an extinction coefficient of 5960 M^{-1} *cm^{-1}.

2.6. Circular dichroism (CD) spectroscopy

CD measurements were performed on Jasco J-720 spectropolarimeter at 20 nm/min scan rate, 8 s time constant and 1 nm step size

in 10 mM phosphate buffer, pH 7.2 at room temperature. The path length was 0.1 cm. Protein concentrations were 4–15 μM for TPPP/p25 forms, 4 μM for SYN and 1 μM for tubulin. The mixtures were incubated for 10 min before recording the spectra. The difference spectrum was obtained by subtracting the spectra of the individual proteins from that of the mixture of two proteins (tubulin and the various TPPP/p25 forms). Mean molar ellipticity per residue (MRE) in degrees square centimeter per decimole was calculated according to the following equation: MRE = $\Theta_m/(10*n*c*l)$, where Θ_m is the measured ellipticity (millidegrees), n is the number of amino acid residues in a protein, c (mol) is the concentration and l (cm) is the path length of the cell. Data from three–five independent measurements were averaged.

2.7. 8-Anilinonaphthalene-1-sulfonic acid (ANS) fluorescence

The fluorescence measurements were performed in 50 mM Tris buffer, pH 7.5 at 25 °C using a Jobin Yvon Fluoromax-3 spectrofluorometer (Jobin Yvon Horiba, Longiumeau, France). A quartz cuvette of 1 cm optical path length and freshly prepared 10 mM ANS stock solution made with ultrapure water were used for each experiment. The fluorophore was excited at 380 nm, emission was monitored from 400 to 600 nm, the slits were adjusted to 2 nm as described in [43]. All measurements were done in triplicate. Data were processed using DataMax software. A blank spectrum without protein was recorded before addition of the wild type or truncated TPPP/p25 forms and $ZnCl_2$. The concentration of ANS, TPPP/p25 forms and $ZnCl_2$ was 50 μM, 2.5 μM and 20 μM, respectively. Three–nine independent measurements were carried out.

2.8. Enzyme-linked immunosorbent assay (ELISA)

The plate was coated with 5 μg/ml (50 μl/well) SYN in phosphate buffered saline as described previously [35]. Briefly, after blocking the wells with bovine serum albumin (BSA), the immobilized proteins were incubated with serial dilutions of wild type or mutant TPPP/p25 forms followed by the addition of TPPP/p25 antibody [16] and the corresponding peroxidase conjugated secondary IgG. In another experimental setup, the plate was coated with 5 μg/ml (50 μl/well) wild type or mutant TPPP/p25 forms, and after blocking the wells with BSA the immobilized proteins were incubated with serial dilutions of polyclonal TPPP/p25 antibody [16] or with serial dilutions of tubulin followed by the addition of tubulin antibody (Sigma T9026) and the corresponding peroxidase conjugated secondary IgG. The bound antibodies were detected using o-phenylenediamine as substrate. The reaction was stopped after 10 min with 1 M H_2SO_4, and the absorbance was read at 490 nm with an EnSpire Multimode Reader (Perkin Elmer). The binding constants (K_d) were evaluated from the saturation curves by non-linear curve fitting assuming single binding site hyperbola model using the Origin 8.0 software.

In the case of the *competitive ELISA*, the plate was coated with 5 μg/ml (50 μl/well) TPPP/p25 in phosphate buffered saline. After blocking the wells with BSA, 0.5 μM SYN preincubated for 30 min in room temperature with 2.5 μM or serial dilutions of TPPP/p25 forms/peptides was added to the immobilized TPPP/p25. The bound SYN was quantified by monoclonal SYN antibody as described above.

2.9. Turbidity measurements

The assembly of tubulin (6 μM) was assessed in polymerization buffer (50 mM 2-(N-morpholino)ethanesulfonic acid buffer pH 6.6 containing 100 mM KCl, 1 mM dithioerythritol, 1 mM $MgCl_2$ and 1 mM ethylene glycol tetraacetic acid) at 37 °C. The tubulin polymerization into microtubules was induced by the addition of 3 μM of the different TPPP/p25 forms. The optical density was monitored at 350 nm by a Cary 100 spectrophotometer (Varian).

2.10. Multinuclear nuclear magnetic resonance (NMR)

Uniformly labeled (^{15}N- and/or ^{13}C–label) DT protein was produced as described previously using M9 minimal medium containing $^{15}NH_4Cl$ and ^{13}C-glucose as sole nitrogen and carbon sources, respectively [10].

For backbone assignment and structural characterization of human *N*- and *C*-terminal free TPPP/p25 protein 1D, 2D and 3D NMR experiments were carried out at 288 K such as ^{1}H-^{15}N-HSQC (8 transients collected using 118 ppm offset; 26 ppm spectral window and incremented in 512 points in the indirect dimension), ^{1}H-^{13}C-HSQC (16 transients with 40 ppm offset and 64 ppm spectral window incremented in 256 points in F1), HNCA, HNCOCA (for both indirect dimension: 8 transients with 50 ppm offset and 64 ppm window for ^{13}C and incremented in 64 × 128 points), HNCACB (16 transients collected with 40 ppm offset and 64 ppm spectral width for ^{13}C and incremented in 64 × 128 points), CCCONH (16 transients collected at 40 ppm offset with 64 ppm spectral window incremented in 64 × 128 points in the indirect dimensions).

Titration with SYN was carried out by recording a series of ^{1}H-^{15}N-HSQC spectra at increasing SYN concentration added to the 800 μM DT sample (8 scans are incremented in 512 points with 26 ppm spectral width at 117 ppm offset), final concentration of DT and SYN was 381 and 327 μM, respectively. SYN perturbation was evaluated by comparing both the ^{1}H and ^{15}N chemical shifts of TPPP/p25 corresponding to 82.5% titration with that of the free protein and calculated as follows: perturbation = $((\Delta\delta^{15}N/6.51)^2 + (\Delta\delta^{1}H/1)^2)^{1/2}$.

2.11. Computational analysis of intrinsic disorder propensity of wild type and mutant forms of human TPPP/p25

We evaluated intrinsic disorder propensity of various TPPP/p25 variants by so-called binary predictors, charge-hydropathy plot (CH-plot) and cumulative distribution function plot (CDF-plot). The CH-plot of a particular sequence is a linear disorder classifier that discriminates proteins with substantial amounts of extended disorder from proteins with globular conformations [44,45]. A CH-plot shows results from a binary disorder predictor and represents an input protein as a 2D graph, in which the mean Kate-Doolittle hydrophobicity and the mean absolute net charge are projected onto the X- and Y-coordinates, respectively. In the corresponding CH-plot, fully structured proteins and fully disordered proteins can be separated by a boundary line. All proteins located above this boundary line are highly likely to be extended, while proteins located below this line are likely to be compact [44,45]. CDF-plot is a cumulated histogram of disordered residues at various disordered scores [45,46]. The cumulated histogram for structured proteins increases faster in the range of smaller disordered scores and then goes flat at larger disordered scores, while the cumulated histogram for disordered proteins increases slightly in the range of lower disordered score but significantly at higher disordered scores. There is a boundary line in the CDF-plot, and the position of a CDF line of a given protein relative to this boundary defines the disorder status of this protein [44].

2.12. Cell culture, transfection and manipulation

HeLa cells (ATCC® CCL-2™, American Type Culture Collection) were grown in Dulbecco's modified eagle medium supplemented with 10% fetal calf serum and 100 μg/ml kanamycin in a humidified incubator at 37 °C with 5% CO_2. Cells were routinely checked for mycoplasma contamination by microscopy using 4,6-diamidino-2-phenylindole (DAPI) staining. Cells were grown on 12-mm-diameter glass coverslips for microscopic analysis. For the co-localization studies HeLa cells were transfected with EGFP-TPPP/p25 or EGFP-CORE constructs, then the cells were stained with a monoclonal antibody against α-tubulin (Sigma T9026); the full length and the truncated TPPP/p25, as well as the microtubule network, were visualized by fluorescence microscopy. Images of the mounted samples were acquired on a Leica DM IL 500 microscope equipped with Leica DFC 395 FX camera and HBO 100w lamp. The equipment software was Leica Application Suite 4.4.0. Chroma UV filter set (No. C40888), Chroma 41028 HQ NB GFP filter set (No. C21116) and Leica filter N2.1 (No. 513832) was used for DAPI, EGFP and Alexa 546 signal acquisition, respectively, using a HCX FL Fluotar 40 ×/0.75 (dry) objective.

For the evaluation of the BiFC signal, HeLa cells were transfected with the mVenus BiFC constructs of TPPP/p25 and SYN (0.3 μg of each plasmid) using Turbofect (Invitrogen) transfection reagent according to the manufacture's protocol. 0,3 μg competitor unlabeled TPPP/p25 plasmid was co-transfected with mVenus BiFC constructs where it mentioned. Nuclei were counterstained with DAPI. Images of the mounted samples were acquired on a Leica DM IL 500 microscope as above. Chroma UV filter set (No. C40888) and Chroma 41028 Y GFP filter set (No. C2117) was used for DAPI and Venus signal acquisition, respectively.

For image analysis, the pictures were taken under constant exposure parameters. The determination of the BiFC signal (green fluorescence) was performed by using the Analyze, Measure option of the National Institutes of Health ImageJ software using the original grayscale pictures. The whole territory of each cell was outlined by the Freehand Line tool and integrated pixel densities calculated by multiplying the area of each cell with the corresponding average pixel intensity subtracting the background.

2.13. Statistical analysis

The error bars represent the standard deviation (SD). Comparisons were performed using the unpaired Student's *t*-test and values were considered to be significant if the calculated *p* value was < 0.05 (*).

3. Results

3.1. Generation of deletion mutants of TPPP/p25

Earlier we showed that the ^{147}KAPIISGVTK^{156} segment of the flexible CORE region of TPPP/p25 is involved in the formation of the pathological TPPP/p25-SYN complex, while the 178–187 segment of the *C*-terminus takes part in the formation of the physiological TPPP/p25-tubulin/microtubule complex [35]. Deletion and/or truncated variants and fragments of the human TPPP/p25 were produced by recombinant techniques as described in the Materials and Methods and used for structural and functional studies. The deletions analyzed in this study were focused on the functional regions of TPPP/p25. These TPPP/p25 forms are schematically shown in Fig. 1 and are described in Table 2.

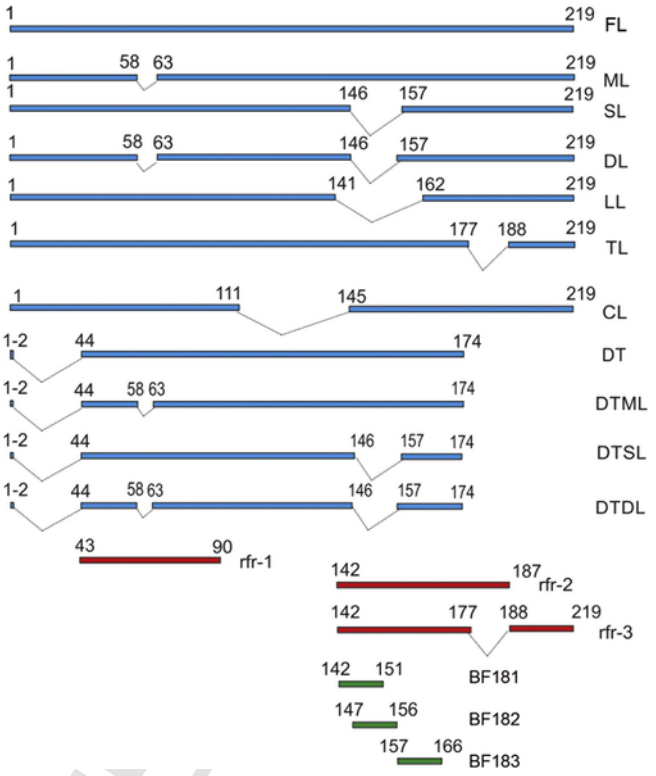

Fig. 1. Scheme of the different TPPP/p25 forms.

3.2. Effect of the TPPP/p25 deletions on the interaction with tubulin/microtubules

We reported that the deletion of the unstructured *N*- and *C*-termini of TPPP/p25 (DT) resulted in significant decrease in the tubulin polymerization promoting activity of this protein [35], and a specific ELISA experiment suggested the role of the 178–187 segment (TL) in the binding of TPPP/p25 to tubulin [35].

Now we performed in vitro studies with deletion mutants and fragments of TPPP/p25 related to its *C*-terminal region, TL, rfr-2 and rfr-3 (see Fig. 1). Previously we showed that the interaction of the full length TPPP/p25 (FL) with tubulin produced a characteristic difference CD spectrum (Fig. 2A) that was significantly reduced due to the truncation of the unstructured *N*- and *C*-termini (DT) [35]. Similar set of experiments was carried out with the TL deletion mutant (Δ178–187) and the rfr-2 and rfr-3 fragments, which include distinct segments of the *C*-terminal region of TPPP/p25 (cf. Fig. 1). As illustrated in Fig. 2B, in the case of the fragments virtually no CD difference signals were evolved, whereas in the case of TL a reduced difference spectrum was observed. ELISA experiments with the *C*-terminal mutants are shown in Fig. 2C. While the TL deletion mutant behaved similarly as the full-length TPPP/p25 (FL), the two *C*-terminal fragments of this protein displayed significantly reduced (rfr-3) or no (rfr-2) binding capacity toward tubulin. The turbidity measurements (Fig. 2D) underlined the results of the binding studies, namely that the TL deletion mutant maintained the tubulin polymerization promoting activity, whereas the fragments failed to induce tubulin polymerization. Finally, experiments carried out with a mutant of the CORE region (SL, see Fig. 1) involved in the formation of the pathological TPPP/p25-SYN complex [35], proved that the deletion of this region caused only modest, if any, reduction in the association of the

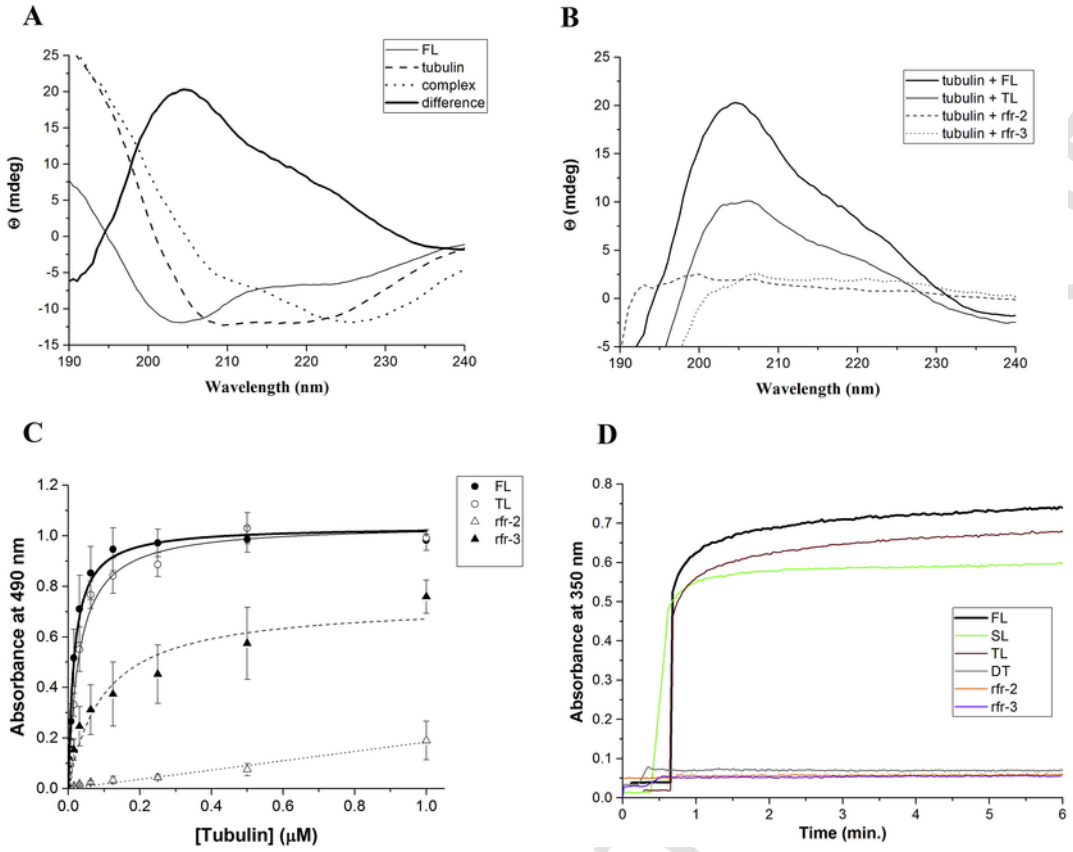

Fig. 2. Interaction of tubulin with TPPP/p25 deletion mutants affecting the *C*-terminal region. (A–B) Difference CD spectra of TPPP/p25 forms and tubulin. Difference ellipticity was calculated by subtracting the ellipticities of tubulin and the TPPP/p25 forms from that measured with their mixtures. The concentration of tubulin, TPPP/p25, TL, rfr-2 and rfr-3 was 1, 5, 5, 15 and 10 μM, respectively. (A) Spectrum of FL (solid line) and tubulin (dashed line), complex spectrum (dotted line), difference spectrum (bold line), average of three independent experiments. (B) Difference spectrum of FL (bold line), TL (solid line), rfr-2 (dashed line), rfr-3 (dotted line), average of three independent experiments. (C) ELISA experiment. The plate was coated with the various TPPP/p25 forms, then it was incubated with tubulin at different concentrations. The bound tubulin was detected by tubulin antibody as described in the Materials and Methods. FL (●), TL (○), rfr-2 (Δ), rfr-3 (▲). The results are presented as means ± the standard deviation (SD). The binding affinities of the distinct TPPP/p25 forms to tubulin evaluated by curve fitting assuming simple hyperbolic saturation were found to be 16.4 ± 1.4 (FL, n = 11), 29.8 ± 2.7 (TL, n = 3), and 97.0 ± 29.9 (rfr-3, n = 4) nM, respectively. For rfr-2, n = 3. (D) The tubulin polymerization promoting potency of the TPPP/p25 forms followed by turbidimetry. The polymerization of 6 μM tubulin to microtubules was induced by the addition of 3 μM of each TPPP/p25 form. A representative experiment is shown, n = 3–8.

TPPP/p25 with tubulin (Fig. 2D). Therefore, the physiological interface seems to be, indeed, distinct from the pathological one within the CORE region.

3.3. NMR spectroscopy of the SYN binding to the CORE region of TPPP/p25

Both the co-enrichment and the co-localization of TPPP/p25 and SYN were detected in brain inclusions of patients suffering from Parkinson's disease and multiple system atrophy [16]; the direct associations of the two disordered proteins were characterized at molecular and cellular levels [35,36]. In addition, the CORE region (45–174 aa) of TPPP/p25, specifically the 147–156 aa segment of this protein, was suggested by ELISA experiments to be localized at the interface in the TPPP/p25-SYN pathological complex [35]. However, the synthesized 147–156 aa peptide resulted in only partial inhibition of its assembly. In order to assign the amino acid residues involved in the formation of the pathological complex, multinuclear NMR studies of the ^{15}N-labeled CORE segment were performed without and with SYN.

A number of resonance frequencies of the ^{1}H-^{15}N HSQC spectra were sharp and poorly dispersed in the amide region (Fig. 3A), indicating the intrinsically disordered character of these residues. Furthermore, these peaks predominantly fell in the narrow region of 7.8–8.6 ppm ^{1}H, which is typical for the highly flexible proteins, indicating their ability to fluctuate among a multitude of conformational states, therefore, lacking a well-defined single time-average structure [47,48]. The addition of SYN to the ^{15}N-labeled double truncated TPPP/p25 apparently did not cause global structural changes of the protein. However, the addition of SYN led to significant changes in the chemical shifts of amides of some TPPP/p25 residues, indicating that there was an alteration of the chemical environment around these TPPP/p25 groups involved in the direct contact with SYN. Larger perturbation than the arbitrarily defined cut-off signal (0.017 ppm) was detected for the assigned residues within the 110–122 aa region, at the residues 110–111, 114, 117, 121–122 of the CORE segments that corresponds to the 151–164 region of the full length protein (Fig. 3B). Furthermore, a new segment, 18–21 (59–62 aa in the full length) was identified as another SYN binding region. These findings indicate the complex nature of the interaction mode of the truncated TPPP/p25 with SYN. Therefore, it can be concluded, that at least two separated domains of the CORE segment of TPPP/p25 could be involved in the SYN binding.

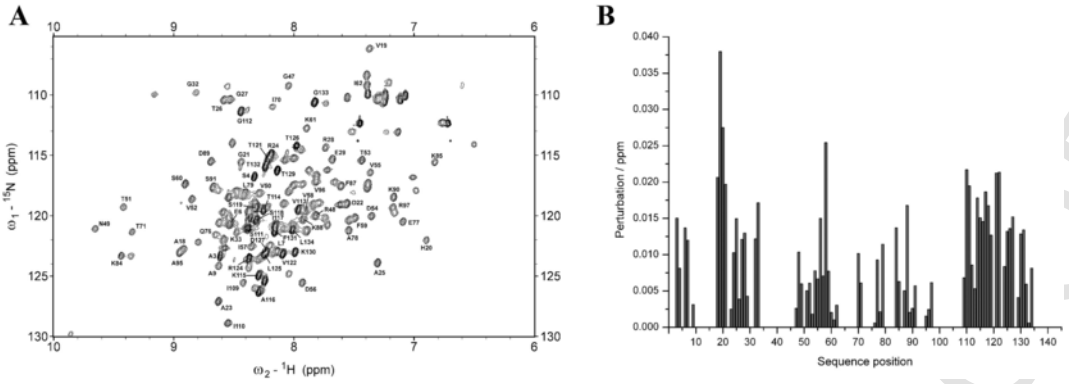

Fig. 3. Multinuclear NMR spectroscopy of the CORE TPPP/p25 with added SYN. (A) Backbone H—N cross-peaks. (B) Residues 18–21, 58, 110–111, 114, 117, 121–122 aa display larger than 0.017 ppm threshold shift due to the addition of SYN. Final concentration of DT and SYN was 381 and 327 μM, respectively.

3.4. Effect of the deletions in the CORE segment of TPPP/p25 on its association with SYN

Previously we suggested the involvement of the 147–156 segment of the CORE region in the SYN binding [35]. Now the multinuclear NMR analysis underlined this observation and suggested the involvement of the 59–62 segment (ML) in the constitution of the interface of the TPPP/p25-SYN complex (see Fig. 3). Accordingly, double deletion mutants of the full length TPPP/p25 (DL) and the CORE variant (DTDL) were designed, expressed, isolated, and their interactions with SYN were characterized by ELISA as follows: SYN was immobilized on ELISA plate followed by the addition of TPPP/p25 variants at different concentrations. Complex formation was detected by the TPPP/p25 antibody as described in the Materials and Methods. Fig. 4A illustrates that the polyclonal TPPP/p25 antiserum recognized the mutant TPPP/p25 species, and could be used for quantification of the hetero-association between TPPP/p25 and SYN.

The double deletion mutant of the full length TPPP/p25 (DL) displayed decreased, but comparable binding affinity to the SYN as the wild type protein (FL) (Fig. 4B). However, the double deletion mutant of the CORE variant (DTDL) virtually failed to associate to SYN (Fig. 4B); this termini-free form, the CORE with double deletion is the single variant of TPPP/p25 mutants that did not bind to SYN. This finding revealed the contribution of the unstructured tails of TPPP/p25 to form the pathological complex.

In fact, we tested several single deletion mutants of both the FL and DT (CORE) variants such as ML, SL, LL, CL, DTML and DTSL (cf. Table 2 and Fig. 1 for the identification of the TPPP/p25 variants). As shown in Fig. 4B, no or limited reduction in the SYN binding was detected. It is also worth mentioning that the fragments involving the 147–156 segment (rfr-2 and rfr-3) failed to associate to SYN (Fig. 4B). These results highlighted the mutual association of the distinct TPPP/p25 segments to SYN.

The binding affinities of the deletion/truncated TPPP/p25 mutants to SYN were evaluated by curve fitting assuming simple hyperbolic saturation. Analysis of these data revealed that the various deletion mutants can be arranged in the following order according to their SYN binding affinities:

FL ~ ML>LL
~ CL
~ DL>SL>>**DT**>DTML
~ DTSL>>>**DTDL**~**rfr−2**~**rfr−3**

Rather interestingly, we noticed that the association of the two disordered proteins, TPPP/p25 and SYN, did not result in the formation of a difference CD spectrum (Fig. 4C) in spite of their hetero-association, while in the case of the interaction of the disordered TPPP/p25 and the globular tubulin extensive spectral changes as difference ellipticity spectrum could be detected (cf. Fig. 2A). These findings, where the disordered TPPP/p25 obviously possesses distinct conformational states by interacting with SYN or tubulin, are indicative of the *chameleon* nature of TPPP/p25 as well.

3.5. Deletion-derived conformational changes of TPPP/p25

Next, the conformational properties of the deletion and/or truncated mutants and fragments of TPPP/p25 were characterized as compared with the full length protein (cf. Fig. 1). To this end, we utilized both experimental and computational approaches and analyzed various TPPP/p25 constructs by CD and ANS spectroscopy as well as by various prediction software products developed for characterization of IDPs.

TPPP/p25 displayed a CD spectrum with high random coil content characteristic for the highly disordered proteins [7,49]. As shown in Fig. 5A, in the case of the full length TPPP/p25 (FL) and its deletion mutants (ML, SL, DL, LL, TL) the minimum is at 205 nm independently of the nature of the deletions. However, the truncation of the disordered *N*- and *C*-terminal tails (DT) produced a partially folded protein as evidenced by the altered minimum and the significant changes in the ratio of the ellipticities at the minimum and 222 nm. This feature seemed to be maintained in the case of the double truncated double deletion form (DTDL) that appeared as an inactive variant with respect to SYN binding. In contrast to the truncation mutants (DT without and with deletions), the CD spectra of the fragments (rfr-2 and rfr-3) of TPPP/p25 displayed exclusively random coil structure corresponding to an unfolded polypeptide chain (Fig. 5A).

Since the binding of ANS to the hydrophobic regions of proteins is coupled with an enhanced fluorescence intensity and a pronounced blue shift of the fluorescence maximum, this technique is a unique

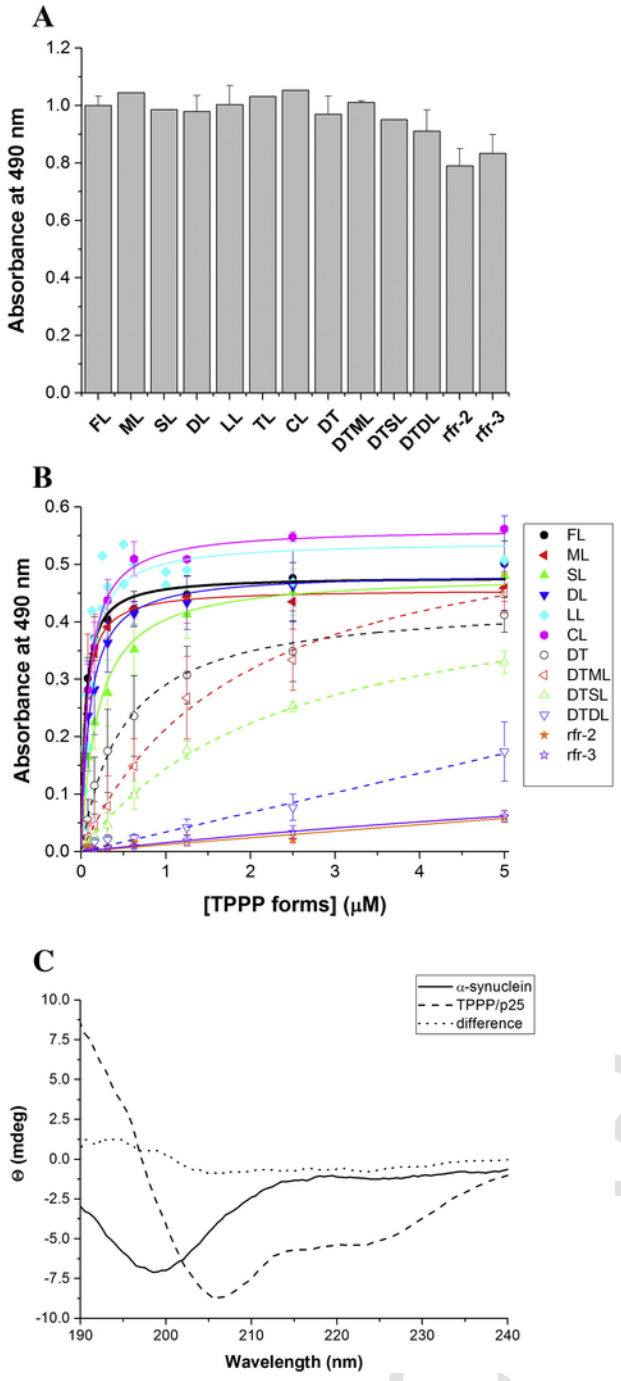

Fig. 4. Interaction of SYN with TPPP/p25 deletion mutants affecting the CORE region. (A) Polyclonal TPPP/p25 antiserum recognizes the various mutant forms as detected by ELISA. The plate was coated with the different TPPP/p25 species, then polyclonal TPPP/p25 antiserum was added at saturation value. The results are presented as means ± the standard deviation (SD). The values were normalized with respect to that measured for the FL. (B) Binding of SYN to the various TPPP/p25 mutants determined by ELISA experiment. The plate was coated with SYN, then it was incubated with the various TPPP/p25 forms at different concentrations. The binding affinities of the distinct TPPP/p25 forms to SYN evaluated by curve fitting assuming simple hyperbolic saturation were found to be 48.9 ± 6.7 (FL, n = 7), 51.3 ± 2.7 (ML, n = 4), 194 ± 22 (SL, n = 4), 99.5 ± 12 (DL, n = 3), 77.3 ± 13 (LL, n = 3), 84.3 ± 6.2 (CL, n = 2), 499 ± 44 (DT, n = 6), 1865 ± 217 (DTML, n = 4) and 2392 ± 209 (DTSL, n = 4) nM, respectively. The results are presented as means ± the standard deviation (SD). For rfr-2 and rfr-3, n = 2. (C) Difference CD spectrum of TPPP/p25 form and SYN. Difference ellipticity was calculated by subtracting the ellipticities of SYN and TPPP/p25 from that measured with their mixtures. The concentration of SYN and TPPP/p25 was 4 and 4 μM, respectively. Spectrum of FL (dashed line) and SYN (solid line), difference spectrum (dotted line), average of three independent experiments.

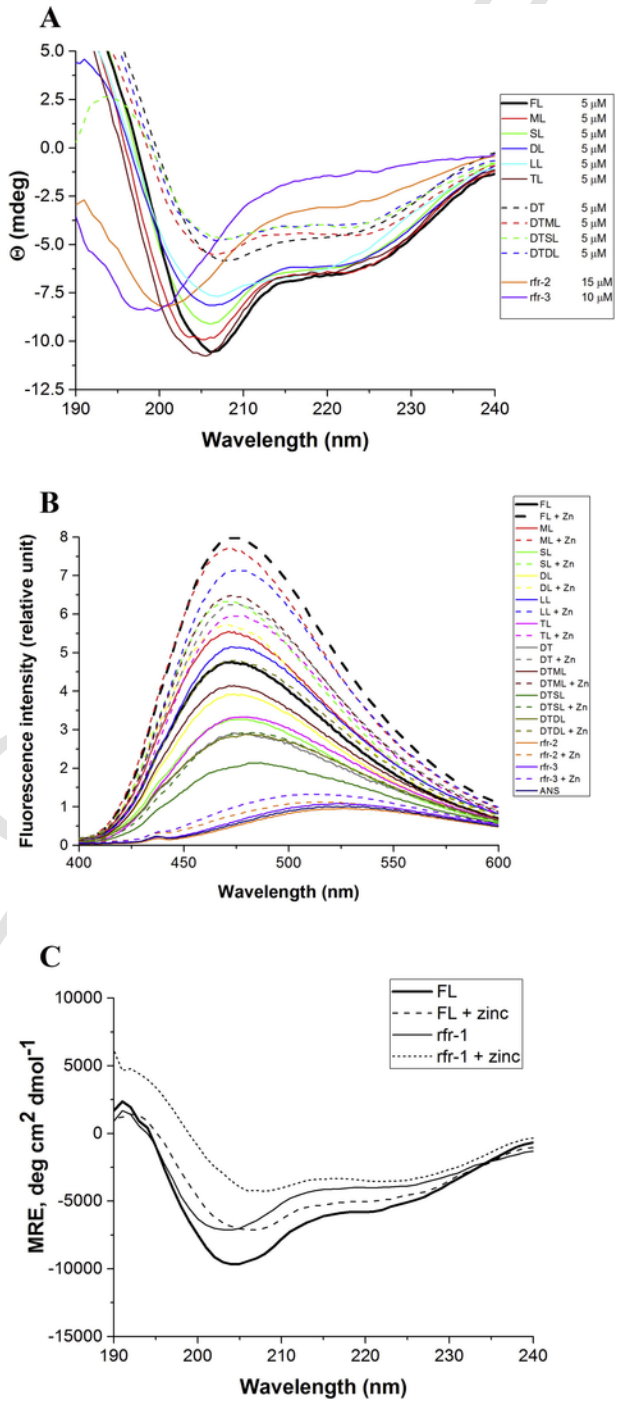

Fig. 5. Effect of the different mutations on the structural characteristics of TPPP/p25. (A) Far-UV CD spectra of the various TPPP/p25 forms. Average of three–five independent experiments (B) ANS fluorescence spectroscopy. Representative emission spectra are shown. The concentration of ANS and protein was 50 μM and 2.5 μM, respectively; n = 3–9 experiments. (C). Normalized far-UV CD spectra of TPPP/p25 and rfr-1 species without and with 200 μM zinc. FL (bold line) with zinc (solid line), rfr-1 (dashed line) with zinc (dotted line), average of three independent experiments.

test for identification of the molten globule state [50,51]. Previously, we detected these effects upon addition of ANS to the full-length TPPP/p25 as well. We reported the suitability of the ANS assay for the characterization of the effect of the bivalent zinc ion on the protein [43], because TPPP/p25 contains a zinc-finger region ($His^{61}(X)_{10}His^{72}(X)_7Cys^{80}(X)_2Cys^{83}$) responsible for the specific binding of this cation [43]. Now we tested the effect of the various mutants and fragments on the ability of TPPP/p25 to undergo zinc-induced local structural alterations. Note that the His and Cys residues of the zinc-finger motif are not affected by the deletions, except in the cases of ML and DL, where His^{61} is missing. Deletions of one or more segments with different lengths produced relatively minor decrease in the ANS signal; significant change appeared in the case of the SL (Δ147–156) and the double truncated (CORE) forms (Fig. 5B, Additional file 1). The addition of zinc ion significantly increased the ANS fluorescence intensity in all truncated forms as well as in the full length TPPP/p25 except in the variants (ML, DL, DTML, DTDL) where His^{61} was deleted. On the basis of ANS data the hydrophobicity of the TPPP/p25 variants is the following: (Fig. 5B, Additional file 1):

DTSL <DTDL
~ SL
~ DT<TL
~ DL<DTML<FL
~ LL<ML,

with zinc DTSL <DTDL <DT
~ DL
~ TL
~ SL<DTML
~ LL<ML
~ FL

The finding that the zinc-induced structural changes were restricted to the zinc-finger region is supported by the far-UV CD data (Fig. 5C). We found that the 43–90 fragment of TPPP/p25 (rfr-1) with the zinc finger region displayed similar structural change by the addition of zinc as the full length TPPP/p25 indicating that a well-defined binding domain can be maintained in a well-defined segment/fragment of the disordered protein, no "chameleon effect" has to be assumed to elucidate the phenomenon.

Next, we conducted a multiparametric computational analysis of various deletion and truncation mutants of TPPP/p25 in order to understand how sequence alterations would affect intrinsic disorder propensity of this protein. Results of the evaluation of per-residue intrinsic disorder predisposition of various TPPP/p25 variants by a set of the predictors of PONDR family and the effect of mutations and truncations on the disorder-based interactivity of this protein are summarized in Additional file 2. Although we used several unrelated per-residue disorder predictors sensitive to different sequence attributes, the outputs of these different computational tools are typically in agreement with each other (see Additional files 2, 3). Furthermore, these computational analyses generally agreed with the experimental data and clearly showed that the full length TPPP/p25 is a highly disordered protein. Deletion mutations did not have a significant effect on the disorder status of this protein, whereas truncation of its *N*- and *C*-termini (as well as the subsequent deletions within this truncated form) made TPPP/p25 more ordered [35].

We also looked at the intrinsic disorder propensities of the wild type human TPPP/p25 and its variants using binary disorder predictors that classify the entire protein as ordered or disordered as a whole, and the results of this analysis are shown in Fig. 6. CDF analysis is shown in Fig. 6A. It summarizes the per-residue disorder predictions by plotting PONDR scores against their cumulative frequency, which allows ordered and disordered proteins to be distinguished on the basis of the distribution of prediction scores [44]. At any given point on the CDF curve, the ordinate gives the proportion of residues with a PONDR score less than or equal to the abscissa. The optimal boundary that provided the most accurate order-disorder classification was shown to represent seven points located in the 12th through 18th bins [44]. Thus, for CDF analysis, order-disorder classification is based on whether a CDF curve of a given protein is above or below a majority of boundary points. Fig. 6A shows that the full-length TPPP/p25 and all its deletion mutants were predicted to be disordered, since their CDF curves were located below the boundary. On the other hand, CDF curves corresponding to the truncated TPPP/p25 and its deletion variants were all located in close vicinity to the boundary line, suggesting that the overall disorder status of these forms of TPPP/p25 is "undecided".

Fig. 6B represents a CH-plot, where the absolute mean net charges of proteins (R) are plotted against their mean hydropathy (H) and which shows that ordered and disordered proteins tend to occupy two different areas within the charge-hydrophobicity phase space, being separated by an estimated boundary line, $R = 2.785*H - 1.151$ [45]. It is known that the CH-plot is able to discriminate proteins with substantial amounts of extended disorder (random coils and pre-molten globules, which are located above the boundary) from proteins with globular conformations (molten globule-like and ordered globular proteins, which are positioned below the boundary) based on charge and hydropathy of their sequences [44]. Fig. 6B shows that the full-length TPPP/p25 protein and its deletion mutants (except to TL, Δ178–187) were located above the boundary separating compact proteins and extended disordered proteins and were, therefore, predicted to be disordered. On the other hand, TL variant, truncated TPPP/p25, and all its deletion variants were predicted to be compact, being located below the boundary.

Concluding, according to the results of CDF-plot (Fig. 6A) and CH-plot analysis (Fig. 6B), the full-length TPPP/p25 protein and its deletion mutants were all predicted to be disordered as a whole. On the other hand, CORE of TPPP/p25 and its deletion mutants were predicted to be compact proteins with "undecided" disorder status.

3.6. Chameleon nature and druggability of the disordered TPPP/p25

The data obtained for the deletion mutants and fragments of TPPP/p25 and the interactions of these variants with the physiological (tubulin) and pathological (SYN) partners are summarized in Table 3.

On the basis of these data it can be concluded that the deletions of various central regions virtually did not affect the interactions of TPPP/p25 with either tubulin or SYN, whereas the truncation of the unstructured termini did have a strong influence on the binding and function of this protein to tubulin and SYN (cf. Fig. 2C and D). Our studies clearly indicated that the deletions of internal segments of the full length TPPP/p25 involved in the hetero-associations could be replaced by other segments or conformations adapted by the mutations themselves and/or due to the association with SYN. This is a plausible explanation for the interpretation of the binding and functional re-

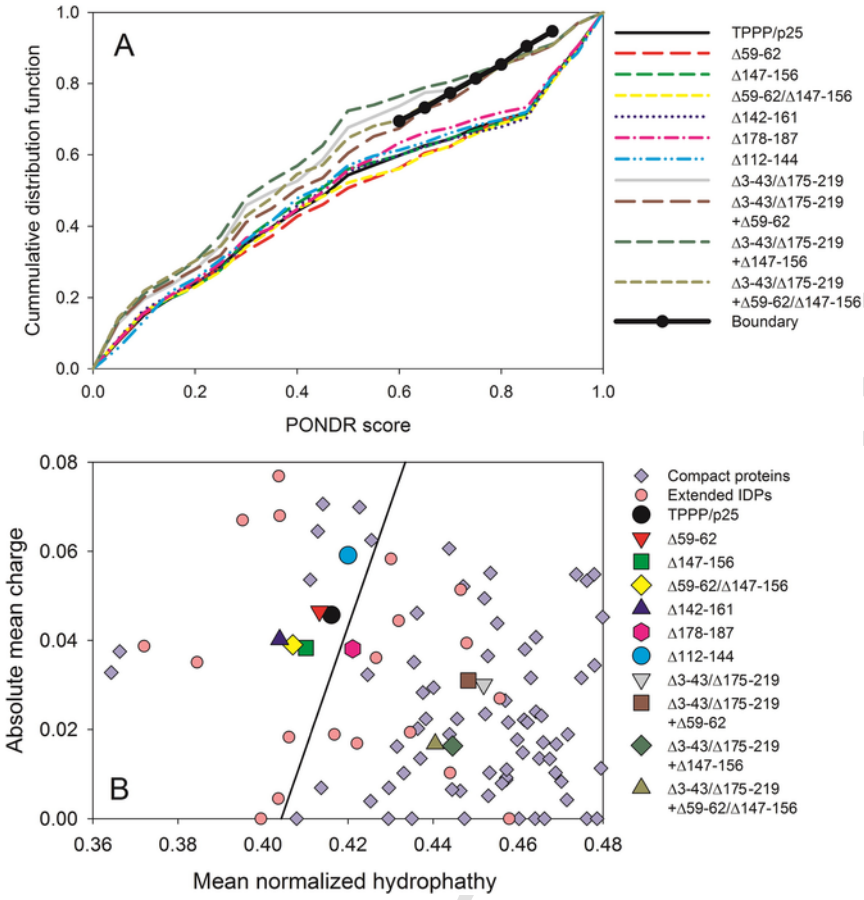

Fig. 6. Evaluation of disorder propensities of TPPP/p25 and its variants by binary disorder predictors. (A) CDF analysis of whole protein order and disorder. CDF curves for TPPP/25 and its various forms are shown as colored lines, and the order-disorder boundary is shown as a black line. (B) CH-plot analysis of whole protein order and disorder. Data for TPPP/25 and its various forms are shown as differently colored symbols. Data for compact ordered proteins and known extended disordered proteins are shown as light-blue diamonds and light-pink circles, respectively. The order-disorder boundary is shown as a black line.

sults obtained with mutants; however, one can suggest other ones to be considered. Given that both proteins are intrinsically disordered, the proteins could tangle/slide on each other displaying interactions. The interaction between the positively and negatively charged TPPP/p25 and SYN, respectively, indeed, is not necessarily conformational specific, it could be driven by side chain salt bridges in spite of the fact that all binding experiments were performed at physiological salt concentration. Therefore, in the case of the TPPP/p25-SYN complex more than one segment of these disordered proteins could be involved in the construction of interface of the assembled proteins that cooperatively can affect the specificity and/or affinity the hetero-association.

3.7. Validation of the interface for drug targeting

To validate the segment of the full-length TPPP/p25 relevant at pathological conditions as a potential drug target, competitive ELISA experiments were carried out. This in vitro assay with human recombinant proteins, TPPP/p25 and SYN, is a well-established approach for screening interaction inhibitors. We used recombinant and synthesized fragments of TPPP/p25 that are expected to function according to their direct binding potency.

In the competitive ELISA assay, the TPPP/p25 variants used as competitors were premixed with SYN at constant concentration, then added to the full-length TPPP/p25 immobilized on the ELISA plate. The inhibitory effect of the competitors on the interaction of SYN with the immobilized TPPP/p25 was detected by a SYN antibody as described in the Materials and Methods. As shown in Fig. 7A, mutants of the full length TPPP/p25 (FL) displayed similar inhibitory potency as the control, while the double truncated form (DT) and its mutants, specifically the one with the deletions of the 59–62 and 147–156 segments (DTDL), showed very low inhibitory activity.

Fig. 7B illustrates the concentration-dependent inhibitory effects of the double truncated forms (DT, DTDL) and fragments. While 10 μM DT produced 80% inhibition, DTDL displayed only 20% inhibitory activity indicating that multiple deletions (terminals and within the CORE segment) are needed to eliminate the interaction of TPPP/p25 with SYN.

The inhibitory (competitive) potency of synthetized peptides of TPPP/p25, BF181, BF182 and BF183 (see Fig. 1) used previously in interaction studies [35] were also tested in a similar set of ELISA experiments. Fig. 7B shows that only the BF182 peptide corresponding to the 147–156 segment inhibited significantly the binding of SYN to the full-length TPPP/p25. These results further corroborated that the 10 aa segment of TPPP/p25 within the flexible CORE region plays a role in the formation of the pathological TPPP/p25-SYN complex, in addition that the competitive ELISA is a simple, powerful assay to screen potential anti-Parkinson drugs.

Table 3
Structural and functional features of the deletion mutant and fragments of TPPP/p25.

	FL	ML	SL	DL	LL	TL	CL
Sequence	1–219	1–58, 63–219	1–146, 157–219	1–58, 63–146, 157–219	1–141, 162–219	1–177, 188–219	1–111, 145–219
Characteristics							
CH-plot prediction	Disordered	Disordered	Disordered	Disordered	Disordered	Ambiguous	Disordered
CD spectrum	Random coil	Random coil	Random coil	Random coil	Random coil	Random coil	
CD + zinc	Yes						
ANS	Yes	Yes	Reduced	Yes	Yes	Yes	
ANS + zinc	Increase	Slight increase	Increase	Slight increase	Slight Increase	Increase	
pAb	Yes	Yes	Yes	Yes	Yes	Yes	Yes
Interaction with tubulin/MT							
ELISA	Yes	Yes	Yes	Yes	Yes	Yes	Yes
CD	Yes	Yes	Yes	Reduced	Yes	Reduced	
Turbidity	Yes	Yes	Yes	Yes	Yes	Yes	
Interaction with SYN							
ELISA	Yes	Yes	Yes	Yes	Yes		Yes
competitive ELISA	Yes	Yes	Yes	Yes	Yes		

	DT	DTML	DTSL	DTDL
Sequence	1–2, 44–174	1–2, 44–58, 63–174	1–2, 44–146, 157–174	1–2, 44–58, 63–146, 157–174
Characteristics				
CH-plot prediction	Compact	Compact	Compact	Compact
CD spectrum	Partially folded	Partially folded	Partially folded	Partially folded
CD + zinc				
ANS	Reduced	Yes	Reduced	Reduced
ANS + zinc	Increase	Slight increase	Increase	Slight increase
pAb	Yes	Yes	Yes	Yes
Interaction with tubulin/MT				
ELISA				
CD	No [35]			
Turbidity	No [35]			
Interaction with SYN				
ELISA	Reduced	Reduced	Reduced	No
Competitive ELISA	Reduced	Reduced	Reduced	No

	rfr-1	rfr-2	rfr-3
Sequence	43–90	142–187	142–177, 188–219
Characteristics			
CH-plot prediction			
CD spectrum	Random coil	Unfolded	Unfolded
CD + zinc	Yes		
ANS		No	No
ANS + zinc		No	No
pAb		Yes	Yes
Interaction with tubulin/MT			
ELISA		No	Reduced
CD		No	No
Turbidity		No	No
Interaction with SYN			
ELISA		No	No
Competitive ELISA			

3.8. Dynamic association of TPPP/p25 and SYN in HeLa cells

We applied BiFC technology using mVenus vectors (V^N-SYN and V^C-TPPP/p25, Fig. 8A) to verify the dynamic hetero-association of the wild type TPPP/p25 and SYN as relevant pathological forms in HeLa cells.

Previously we reported that in transiently transfected HeLa cells the full length (FL) EGFP-TPPP/p25 were aligned along the microtubule network at relatively low expression level (Fig. 8B, panel a), while the double truncated TPPP/p25 (DT) accordingly to the in vitro experiments distributed within the cytosol (Fig. 8B, panel b) [35].

Applying the BiFC technology now we provided evidence for the in vivo hetero-association of TPPP/p25 and SYN in HeLa cells, in addition we showed that the pathological complex appeared to be co-localized on the microtubule network (Fig. 8B, panel c). To establish the dynamic nature of the hetero-association of the two disordered proteins as well as the availability of this technology for drug testing, unlabeled TPPP/p25 as competitor was also expressed in the HeLa cells (Fig. 8B, panel d). As visualized in the immunofluorescence images, the "competitor" reduced the formation of the TPPP/p25-SYN-derived assembly of the mVenus pair as indicated by the quantification of the green fluorescence signal (Fig. 8C). In addition, the expression of the unlabeled TPPP/p25 (competitor) resulted in the release of the mVenus complex from the microtubule network as well (Fig. 8B, panel d). Indeed, it displayed homogeneous distribution within the cytosol similarly to that obtained with the CORE segment of TPPP/p25 which associates poorly, if at all, to the microtubule network [35]. The results at cellular level underlined the data obtained with human recombinant proteins in vitro, and provided a valuable assay for testing potential anti-Parkinson drugs at cellular level.

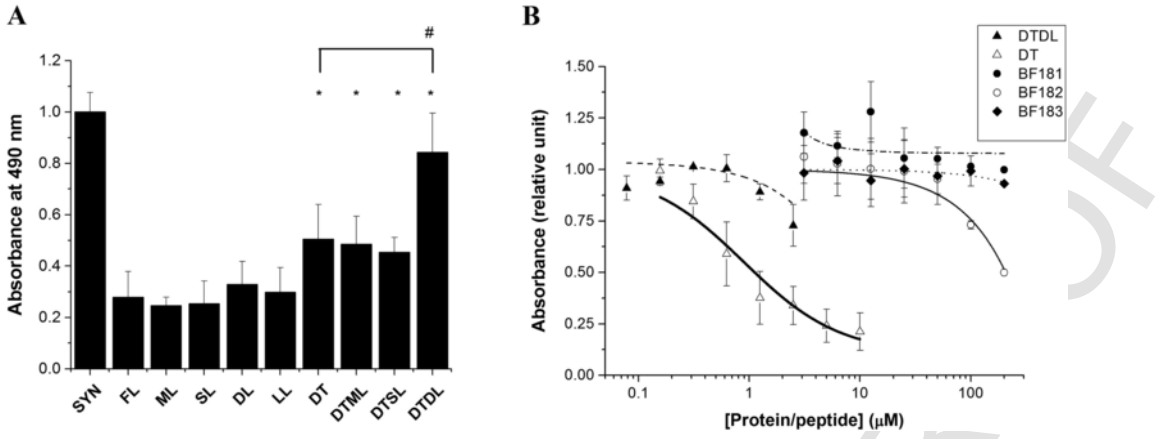

Fig. 7. Effect of the various TPPP/p25 mutants and decapeptides on the SYN-TPPP/p25 interaction determined by competitive ELISA. The plate was coated with TPPP/p25, then 0.5 μM SYN preincubated for 30 min in room temperature with 2.5 μM (A) or serial dilutions of TPPP/p25 forms/peptides (B) was added to the immobilized TPPP/p25. The bound SYN was quantified by monoclonal SYN antibody. The ELISA data were normalized with respect to SYN at 0.5 μM without TPPP/p25 mutants or peptides. (A) *Significant difference with respect to SYN with FL, $p = 2.01E\text{-}3$ for DT, $p = 8.34E\text{-}3$ for DTML, $p = 8.17E\text{-}3$ for DTSL and $p = 5.64E\text{-}8$ for DTDL. #Significant difference with respect to SYN with DT, $p = 1.42E\text{-}4$. n = 11 for SYN, n = 9 for FL, n = 3 for ML, n = 4 for SL, n = 6 for DL, n = 5 for LL, n = 8 for DT, n = 5 for DTML, n = 3 for DTSL, and n = 10 for DTDL, respectively. (B) DL (Δ), DTDL (▲), BF182 (○), BF181 (●), BF183 (◆). n = 3 for DT, and n = 2 for DTDL, BF181, BF182 and BF183, respectively. (A–B) The results are presented as means ± the standard deviation (SD).

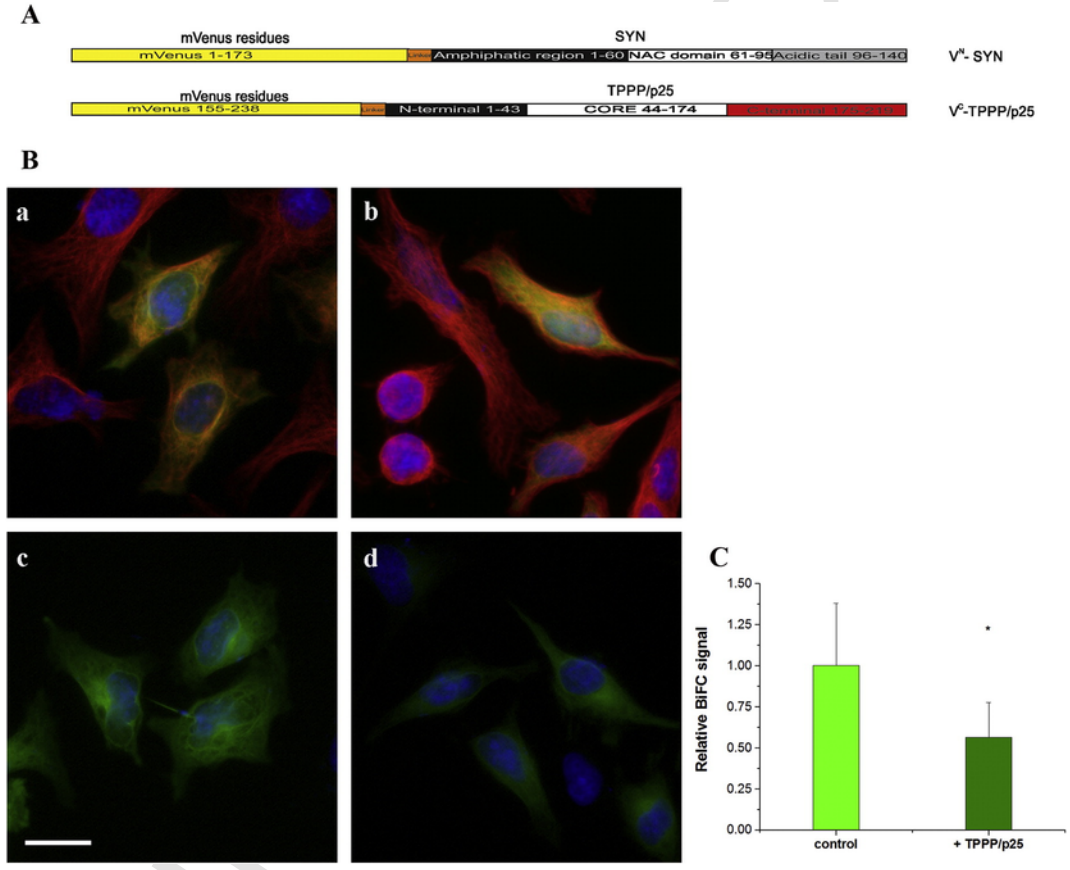

Fig. 8. Dynamic association of TPPP/p25 with SYN on the microtubule network in living HeLa cells as visualized by BiFC technology. (A) Scheme of BiFC constructs for generation of BiFC signal (green) by co-transfection TPPP/p25 and SYN fused to mVenus BiFC constructs (a generous gift of Prof. Péter Várnai; Physiology Department, Semmelweis University, Budapest). (B): (a) Localization of EGFP-TPPP/p25 on the microtubule network (red). (b) Distribution of the EGFP-CORE segment within the cytosol. (c) Alignment of the associated mV^N-SYN and V^C-TPPP/p25 (green). (d) Effect of the unlabeled TPPP/p25 expressed ectopically on the localization of TPPP/p25-SYN interaction-derived mVenus signal. Bar: 10 μm. (C) Quantification of the BiFC signal by detecting the individual cell fluorescence. For densitometric analysis, the images were collected under constant exposure parameters. The mVenus signal intensity was determined by the National Institutes of Health ImageJ software. The whole territory of minimum 30 cells was outlined by the Freehand Line tool and analyzed by taking the sum of the gray values of the pixels in the selection (integrated density) and by subtracting the background. Data were compared by *t*-test, $p = 6.73E\text{-}8$.

4. Discussion

The disordered, highly flexible TPPP/p25 displays both physiological and pathological functions determined by its distinct partner proteins such as tubulin and SYN, respectively [3,35]. This pathophysiological moonlighting feature substantiates high conformational plasticity of this protein that is a characteristic feature of chameleon proteins [19]. In addition, our functional studies proved that the binding segment(s) of the full-length TPPP/p25 could be replaced by other segments resulting in distinct specificities and/or binding affinities. We denoted this intriguing phenomenon as the *neomorphic chameleon* feature.

Rational drug design is based on the well-defined three-dimensional structures of the globular proteins; however, targeting of disordered proteins is a challenging task, since these proteins exist in a highly flexible state forming dynamic structural ensemble without a well-defined 3D structure. For this reason, assignation of the middle (CORE) segment of the full length TPPP/p25 by means of multinuclear NMR has failed [10]. Different strategies have been suggested for targeting these versatile IDP proteins [52,53]. A relevant strategy is "to inhibit interactions with ordered or disordered protein partners" [52]. In fact, there are only a limited number of IDP-related systems studied in drug design; the small molecule inhibitors were mostly identified by experimental screening without considering the mechanism or the toxic side effects of the inhibition [54,55]. Computational unfoldomics is a recently proposed, emerging concept, which identifies metastable structures by simulations coupled with virtual screen of potential inhibitors [53]. In silico high-throughput structure-based docking screen combined with experiments was successfully applied to identify a druggable small molecule which ameliorates SYN-mediated dysfunction in cell models [56]. These studies are promising; however, none of them takes into account the effect of the inhibitors on the physiological functions of IDPs.

Our innovative strategy is based upon the recognition that the physiological binding interface of TPPP/p25 is distinct from the one in the pathological TPPP/p25-SYN complex that could ensure high specificity for drug targeting, e.g., the interface of the pathological complex may serve as an anti-Parkinson drug target (Fig. 9). The specificity is further supported by the unique fact that the assembly of these two disordered hallmarks occurs exclusively at pathological conditions since in normal brain SYN and TPPP/p25 are expressed in neurons [57,58] and oligodendrocytes [9,59], respectively. Previously we showed that TPPP/p25, similarly to SYN, could be taken up by cells from the medium [35]. In addition, both TPPP/p25 [15] and SYN [60] were detected in the cerebrospinal fluid of human patients. Extracellular transmission of these proteins, therefore, is a plausible explanation for the development of pathological inclusions in the case of Parkinson's disease and multiple system atrophy [16,61,62].

We suggested targeting the interface of the pathological complex of multifunctional proteins and validating the binding segment as an innovative strategy for anti-Parkinson drug development. Targeting by competitors/foldamers should impede/destruct the small soluble assemblies, the fatal species in the development of synucleinopathies. The pathological complex has been suggested functioning as an initiator in the etiology of Parkinson's disease and multiple system atrophy [16–18,61,62]. We explored the challenges associated with targeting chameleon proteins using the TPPP/p25-SYN complex as a case study. Our studies exemplify that TPPP/p25, as a chameleon protein with its highly flexible conformation, is known to be involved in distinct CNS diseases [16], thus the innovative strategy supported by these studies could contribute to our understanding the pathomechanism of the Parkinson's and other related diseases.

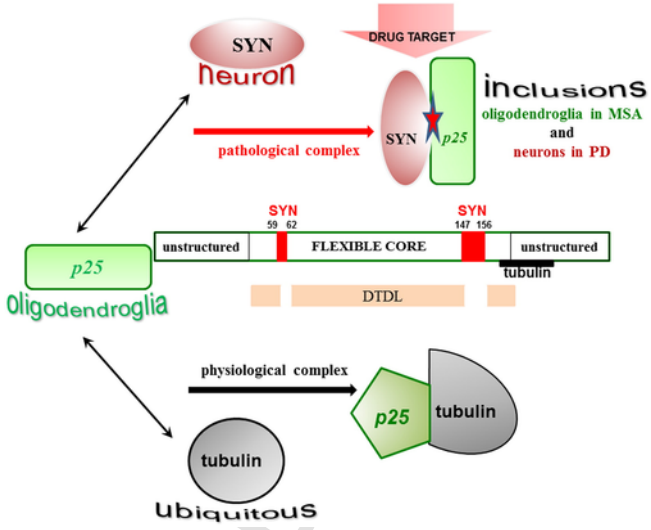

Fig. 9. Distinct interfaces of TPPP/p25 are involved in its hetero-association with tubulin and SYN as physiological and pathological partners, respectively. The interaction of the disordered TPPP/p25 with tubulin results in significant conformational changes; this effect does not manifest itself in the case of its association with SYN. In normal brain the two proteins occur alternatively, in neurons or oligodendrocytes, however, the inclusions due to their pathological assemblies were detected in both cell types in the cases of Multiple System Atrophy (MSA) and Parkinson's disease (PD). Although the deletions within the CORE segments do not diminish the binding of TPPP/p25 mutants to SYN, except in the case of the double truncated double loop mutant (DTDL), due to its chameleon feature; however, multiple segments were identified as potential drug target which are distinct from the segment responsible for the association with tubulin.

Supplementary data to this article can be found online at http://dx.doi.org/10.1016/j.bbadis.2016.09.017.

List of abbreviations

ANS	8-anilinonaphthalene-1-sulfonic acid
BiFC	bimolecular fluorescence complementation
BSA	bovine serum albumin
CH-plot	charge-hydropathy plot
CD	circular dichroism
CDF	cumulative distribution function
DAPI	4,6-diamidino-2-phenylindole
ELISA	enzyme-linked immunosorbent assay
IDP	intrinsically disordered protein
NMR	nuclear magnetic resonance
PCR	polymerase chain reaction
SDS-PAGE	sodium dodecyl sulfate polyacrylamide gel electrophoresis
SYN	α-synuclein
Tris	tris(hydroxymethyl)aminomethane
TPPP/p25	Tubulin Polymerization Promoting Protein

Competing interests

The authors declare that they have no competing interests.

Funding

This work was supported by the European Concerted Research Action COST Action [TD1406 and TD1304]; and the Hungarian

National Scientific Research Fund Grants OTKA [T-101039 and T-112144] to J. Ovádi and [NK101072] to A. Perczel. Support of the MedInProt (MTA) program is acknowledged. The funders had no role in study design, data collection and analysis, decision to publish, or preparation of the manuscript.

Authors' contributions

Tibor Szénási: plan and production of constructs of the TPPP/p25 variants, cloning, expression of proteins, mVenus constructs for the BiFC technology; Judit Oláh: production of labeled protein for the NMR studies, performing and supervising in vitro experiments, data collection and evaluations, responsibility for the research activity including mentorship to MSc and PhD fellows; Adél Szabó: expression and isolation of the recombinant proteins, performing CD, fluorescence and ELISA experiments, data collection and evaluation; Sándor Szunyogh: performing turbidity measurements, data collections, immunocytochemistry with HeLa cells; András Láng: performance of the multinuclear NMR studies, presentation of the published work, evaluation and presentation of the results; András Perczel: creation and presentation of the multinuclear NMR data, acquisition of the financial support for the NMR studies; Attila Lehotzky: planning and implementation of the HeLa cell experiments: cell manipulations, transfections of mVenus BiFC and other constructs, immunocytochemistry, fluorescence microscopy including mentorship to the PhD fellows; Vladimir N. Uversky: planning and conducting of the computational studies, conducting theoretical analysis, interpreting the theoretical findings in relation to the experimental ones; Judit Ovádi: ideas, evolution and coordination of the research aims, planning and execution, acquisition of the financial support for the in vitro and cellular studies.

Transparency document

The Transparency document associated with this article can be found, in online version.

Acknowledgement

We are grateful to Prof. Péter Várnai of the Physiology Department, Faculty of Medicine, Semmelweis University, Budapest, for providing the mVenus BiFC plasmids.

References

[1] C. Conde, A. Caceres, Microtubule assembly, organization and dynamics in axons and dendrites, Nat. Rev. Neurosci. 10 (2009) 319–332.
[2] H. de Forges, A. Bouissou, F. Perez, Interplay between microtubule dynamics and intracellular organization, Int. J. Biochem. Cell Biol. 44 (2012) 266–274.
[3] J. Oláh, N. Tőkési, A. Lehotzky, F. Orosz, J. Ovádi, Moonlighting microtubule-associated proteins: regulatory functions by day and pathological functions at night, Cytoskeleton (Hoboken) 70 (2013) 677–685.
[4] C.J. Jeffery, Moonlighting proteins, Trends Biochem. Sci. 24 (1999) 8–11.
[5] C.J. Jeffery, Proteins with neomorphic moonlighting functions in disease, IUBMB Life 63 (2011) 489–494.
[6] J. Ovádi, Moonlighting proteins in neurological disorders, IUBMB Life 63 (2011) 453–456.
[7] E. Hlavanda, J. Kovács, J. Oláh, F. Orosz, K.F. Medzihradszky, J. Ovádi, Brain-specific p25 protein binds to tubulin and microtubules and induces aberrant microtubule assemblies at substoichiometric concentrations, Biochemistry 41 (2002) 8657–8664.
[8] A. Lehotzky, L. Tirián, N. Tőkési, P. Lénárt, B. Szabó, J. Kovács, J. Ovádi, Dynamic targeting of microtubules by TPPP/p25 affects cell survival, J. Cell Sci. 117 (2004) 6249–6259.
[9] A. Lehotzky, P. Lau, N. Tőkési, N. Muja, L.D. Hudson, J. Ovádi, Tubulin polymerization-promoting protein (TPPP/p25) is critical for oligodendrocyte differentiation, Glia 58 (2010) 157–168.
[10] A. Zotter, A. Bodor, J. Oláh, E. Hlavanda, F. Orosz, A. Perczel, J. Ovádi, Disordered TPPP/p25 binds GTP and displays Mg(2 +)-dependent GTPase activity, FEBS Lett. 585 (2011) 803–808.
[11] N. Tőkési, A. Lehotzky, I. Horváth, B. Szabó, J. Oláh, P. Lau, J. Ovádi, TPPP/p25 promotes tubulin acetylation by inhibiting histone deacetylase 6, J. Biol. Chem. 285 (2010) 17896–17906.
[12] J. Oláh, J. Ovádi, Dual life of TPPP/p25 evolved in physiological and pathological conditions, Biochem. Soc. Trans. 42 (2014) 1762–1767.
[13] M. Preusser, A. Lehotzky, H. Budka, J. Ovádi, G.G. Kovacs, TPPP/p25 in brain tumours: expression in non-neoplastic oligodendrocytes but not in oligodendroglioma cells, Acta Neuropathol. 113 (2007) 213–215.
[14] R. Hoftberger, S. Fink, F. Aboul-Enein, G. Botond, J. Oláh, T. Berki, J. Ovádi, H. Lassmann, H. Budka, G.G. Kovacs, Tubulin polymerization promoting protein (TPPP/p25) as a marker for oligodendroglial changes in multiple sclerosis, Glia 58 (2010) 1847–1857.
[15] O. Vincze, J. Oláh, D. Zadori, P. Klivenyi, L. Vecsei, J. Ovádi, A new myelin protein, TPPP/p25, reduced in demyelinated lesions is enriched in cerebrospinal fluid of multiple sclerosis, Biochem. Biophys. Res. Commun. 409 (2011) 137–141.
[16] G.G. Kovacs, L. Laszlo, J. Kovacs, P.H. Jensen, E. Lindersson, G. Botond, T. Molnar, A. Perczel, F. Hudecz, G. Mezo, A. Erdei, L. Tirian, A. Lehotzky, E. Gelpi, H. Budka, J. Ovádi, Natively unfolded tubulin polymerization promoting protein TPPP/p25 is a common marker of alpha-synucleinopathies, Neurobiol. Dis. 17 (2004) 155–162.
[17] E. Lindersson, D. Lundvig, C. Petersen, P. Madsen, J.R. Nyengaard, P. Hojrup, T. Moos, D. Otzen, W.P. Gai, P.C. Blumbergs, P.H. Jensen, p25alpha stimulates alpha-synuclein aggregation and is co-localized with aggregated alpha-synuclein in alpha-synucleinopathies, J. Biol. Chem. 280 (2005) 5703–5715.
[18] J. Oláh, O. Vincze, D. Virok, D. Simon, Z. Bozsó, N. Tőkési, I. Horváth, E. Hlavanda, J. Kovács, A. Magyar, M. Szűcs, F. Orosz, B. Penke, J. Ovádi, Interactions of pathological hallmark proteins: tubulin polymerization promoting protein/p25, beta-amyloid, and alpha-synuclein, J. Biol. Chem. 286 (2011) 34088–34100.
[19] V.N. Uversky, A protein-chameleon: conformational plasticity of alpha-synuclein, a disordered protein involved in neurodegenerative disorders, J. Biomol. Struct. Dyn. 21 (2003) 211–234.
[20] B.A. Silva, L. Breydo, V.N. Uversky, Targeting the chameleon: a focused look at alpha-synuclein and its roles in neurodegeneration, Mol. Neurobiol. 47 (2013) 446–459.
[21] A. Surguchov, Synucleins: are they two-edged swords?, J. Neurosci. Res. 91 (2013) 161–166.
[22] T.R. Alderson, J.L. Markley, Biophysical characterization of alpha-synuclein and its controversial structure, Intrinsically Disord. Proteins 1 (2013) 18–39.
[23] V.N. Uversky, D. Eliezer, Biophysics of Parkinson's disease: structure and aggregation of alpha-synuclein, Curr. Protein Pept. Sci. 10 (2009) 483–499.
[24] V.N. Uversky, Neuropathology, biochemistry, and biophysics of alpha-synuclein aggregation, J. Neurochem. 103 (2007) 17–37.
[25] B. Fauvet, M.B. Fares, F. Samuel, I. Dikiy, A. Tandon, D. Eliezer, H.A. Lashuel, Characterization of semisynthetic and naturally Nalpha-acetylated alpha-synuclein in vitro and in intact cells: implications for aggregation and cellular properties of alpha-synuclein, J. Biol. Chem. 287 (2012) 28243–28262.
[26] B. Fauvet, M.K. Mbefo, M.B. Fares, C. Desobry, S. Michael, M.T. Ardah, E. Tsika, P. Coune, M. Prudent, N. Lion, D. Eliezer, D.J. Moore, B. Schneider, P. Aebischer, O.M. El-Agnaf, E. Masliah, H.A. Lashuel, Alpha-synuclein in central nervous system and from erythrocytes, mammalian cells, and Escherichia coli exists predominantly as disordered monomer, J. Biol. Chem. 287 (2012) 15345–15364.
[27] D. Eliezer, E. Kutluay, R. Bussell Jr., G. Browne, Conformational properties of alpha-synuclein in its free and lipid-associated states, J. Mol. Biol. 307 (2001) 1061–1073.
[28] V.N. Uversky, J. Li, A.L. Fink, Evidence for a partially folded intermediate in alpha-synuclein fibril formation, J. Biol. Chem. 276 (2001) 10737–10744.
[29] P.H. Weinreb, W. Zhen, A.W. Poon, K.A. Conway, P.T. Lansbury Jr., NACP, a protein implicated in Alzheimer's disease and learning, is natively unfolded, Biochemistry 35 (1996) 13709–13715.
[30] B. Dehay, M. Bourdenx, P. Gorry, S. Przedborski, M. Vila, S. Hunot, A. Singleton, C.W. Olanow, K.M. Merchant, E. Bezard, G.A. Petsko, W.G. Meissner, Targeting alpha-synuclein for treatment of Parkinson's disease: mechanistic and therapeutic considerations, Lancet Neurol. 14 (2015) 855–866.
[31] M. Ozansoy, A.N. Basak, The central theme of Parkinson's disease: alpha-synuclein, Mol. Neurobiol. 47 (2013) 460–465.
[32] H.L. Roberts, D.R. Brown, Seeking a mechanism for the toxicity of oligomeric alpha-synuclein, Biomolecules 5 (2015) 282–305.
[33] B. Winner, R. Jappelli, S.K. Maji, P.A. Desplats, L. Boyer, S. Aigner, C. Hetzer, T. Loher, M. Vilar, S. Campioni, C. Tzitzilonis, A. Soragni, S. Jessberger, H. Mira, A. Consiglio, E. Pham, E. Masliah, F.H. Gage, R. Riek, In vivo

demonstration that alpha-synuclein oligomers are toxic, Proc. Natl. Acad. Sci. U. S. A. 108 (2011) 4194–4199.
[34] E. Valera, G. Monzio Compagnoni, E. Masliah, Review: novel treatment strategies targeting alpha-synuclein in multiple system atrophy as a model of synucleinopathy, Neuropathol. Appl. Neurobiol. 42 (2016) 95–106.
[35] N. Tőkési, J. Oláh, E. Hlavanda, S. Szunyogh, A. Szabó, F. Babos, A. Magyar, A. Lehotzky, E. Vass, J. Ovádi, Identification of motives mediating alternative functions of the neomorphic moonlighting TPPP/p25, Biochim. Biophys. Acta 1842 (2014) 547–557.
[36] S. Szunyogh, J. Oláh, T. Szénási, A. Szabó, J. Ovádi, Targeting the interface of the pathological complex of alpha-synuclein and TPPP/p25, Biochim. Biophys. Acta 1852 (2015) 2653–2661.
[37] S.D. Senanayake, D.A. Brian, Precise large deletions by the PCR-based overlap extension method, Mol. Biotechnol. 4 (1995) 13–15.
[38] I. Palmer, P.T. Wingfield, Preparation and extraction of insoluble (inclusion-body) proteins from Escherichia coli, Curr. Protoc. Protein Sci. (2012) (Unit6 3, Chapter 6).
[39] ExPASy-ProtParam tool, in: http://web.expasy.org/protparam (Accessed 27 May, 2016).
[40] M.M. Bradford, A rapid and sensitive method for the quantitation of microgram quantities of protein utilizing the principle of protein-dye binding, Anal. Biochem. 72 (1976) 248–254.
[41] C.N. Na, S.N. Timasheff, Interaction of vinblastine with calf brain tubulin: multiple equilibria, Biochemistry 25 (1986) 6214–6222.
[42] S.R. Paik, J.H. Lee, D.H. Kim, C.S. Chang, J. Kim, Aluminum-induced structural alterations of the precursor of the non-A beta component of Alzheimer's disease amyloid, Arch. Biochem. Biophys. 344 (1997) 325–334.
[43] A. Zotter, J. Oláh, E. Hlavanda, A. Bodor, A. Perczel, K. Szigeti, J. Fidy, J. Ovádi, Zn(2)+-induced rearrangement of the disordered TPPP/p25 affects its microtubule assembly and GTPase activity, Biochemistry 50 (2011) 9568–9578.
[44] C.J. Oldfield, Y. Cheng, M.S. Cortese, C.J. Brown, V.N. Uversky, A.K. Dunker, Comparing and combining predictors of mostly disordered proteins, Biochemistry 44 (2005) 1989–2000.
[45] V.N. Uversky, J.R. Gillespie, A.L. Fink, Why are "natively unfolded" proteins unstructured under physiologic conditions?, Proteins 41 (2000) 415–427.
[46] A.K. Dunker, J.D. Lawson, C.J. Brown, R.M. Williams, P. Romero, J.S. Oh, C.J. Oldfield, A.M. Campen, C.M. Ratliff, K.W. Hipps, J. Ausio, M.S. Nissen, R. Reeves, C. Kang, C.R. Kissinger, R.W. Bailey, M.D. Griswold, W. Chiu, E.C. Garner, Z. Obradovic, Intrinsically disordered protein, J. Mol. Graph. Model. 19 (2001) 26–59.
[47] I. Radhakrishnan, G.C. Perez-Alvarado, D. Parker, H.J. Dyson, M.R. Montminy, P.E. Wright, Solution structure of the KIX domain of CBP bound to the transactivation domain of CREB: a model for activator:coactivator interactions, Cell 91 (1997) 741–752.
[48] A. Sillen, P. Barbier, I. Landrieu, S. Lefebvre, J.M. Wieruszeski, A. Leroy, V. Peyrot, G. Lippens, NMR investigation of the interaction between the neuronal protein tau and the microtubules, Biochemistry 46 (2007) 3055–3064.
[49] O. Vincze, N. Tőkési, J. Oláh, E. Hlavanda, Á. Zotter, I. Horváth, A. Lehotzky, L. Tirián, K.F. Medzihradszky, J. Kovács, F. Orosz, J. Ovádi, Tubulin polymerization promoting proteins (TPPPs): members of a new family with distinct structures and functions, Biochemistry 45 (2006) 13818–13826.
[50] G.V. Semisotnov, N.A. Rodionova, O.I. Razgulyaev, V.N. Uversky, A.F. Gripas, R.I. Gilmanshin, Study of the "molten globule" intermediate state in protein folding by a hydrophobic fluorescent probe, Biopolymers 31 (1991) 119–128.
[51] S.S. Leal, C.M. Gomes, Studies of the molten globule state of ferredoxin: structural characterization and implications on protein folding and iron-sulfur center assembly, Proteins 68 (2007) 606–616.
[52] P. Joshi, M. Vendruscolo, Druggability of intrinsically disordered proteins, Adv. Exp. Med. Biol. 870 (2015) 383–400.
[53] J. Wang, Z. Cao, L. Zhao, S. Li, Novel strategies for drug discovery based on intrinsically disordered proteins (IDPs), Int. J. Mol. Sci. 12 (2011) 3205–3219.
[54] Y. Zhang, H. Cao, Z. Liu, Binding cavities and druggability of intrinsically disordered proteins, Protein Sci. 24 (2015) 688–705.
[55] S.J. Metallo, Intrinsically disordered proteins are potential drug targets, Curr. Opin. Chem. Biol. 14 (2010) 481–488.
[56] G. Toth, S.J. Gardai, W. Zago, C.W. Bertoncini, N. Cremades, S.L. Roy, M.A. Tambe, J.C. Rochet, C. Galvagnion, G. Skibinski, S. Finkbeiner, M. Bova, K. Regnstrom, S.S. Chiou, J. Johnston, K. Callaway, J.P. Anderson, M.F. Jobling, A.K. Buell, T.A. Yednock, T.P. Knowles, M. Vendruscolo, J. Christodoulou, C.M. Dobson, D. Schenk, L. McConlogue, Targeting the intrinsically disordered structural ensemble of alpha-synuclein by small molecules as a potential therapeutic strategy for Parkinson's disease, PLoS One 9 (2014), e87133.
[57] L. Maroteaux, J.T. Campanelli, R.H. Scheller, Synuclein: a neuron-specific protein localized to the nucleus and presynaptic nerve terminal, J. Neurosci. 8 (1988) 2804–2815.
[58] C.A. Bates, W. Zheng, Brain disposition of alpha-synuclein: roles of brain barrier systems and implications for Parkinson's disease, Fluids Barriers CNS 11 (2014) 17.
[59] M. Takahashi, K. Tomizawa, S.C. Fujita, K. Sato, T. Uchida, K. Imahori, A brain-specific protein p25 is localized and associated with oligodendrocytes, neuropil, and fiber-like structures of the CA hippocampal region in the rat brain, J. Neurochem. 60 (1993) 228–235.
[60] O. Marques, T.F. Outeiro, Alpha-synuclein: from secretion to dysfunction and death, Cell Death Dis. 3 (2012), e350.
[61] K. Ota, M. Obayashi, K. Ozaki, S. Ichinose, A. Kakita, M. Tada, H. Takahashi, N. Ando, Y. Eishi, H. Mizusawa, K. Ishikawa, Relocation of p25alpha/tubulin polymerization promoting protein from the nucleus to the perinuclear cytoplasm in the oligodendroglia of sporadic and COQ2 mutant multiple system atrophy, Acta Neuropathol. Commun. 2 (2014) 136.
[62] K.A. Jellinger, G.K. Wenning, Multiple system atrophy: pathogenic mechanisms and biomarkers, J. Neural Transm. 123 (2016) 555–572.